CARDIFF UNIVERSITY
PRIFYSGOL CAERDYDD

ORCA – Online Research @ Cardiff

This is an Open Access document downloaded from ORCA, Cardiff University's institutional repository:https://orca.cardiff.ac.uk/id/eprint/149366/

This is the author's version of a work that was submitted to / accepted for publication.

Citation for final published version:

Quaglia, Roberto , Powell, Jeffrey R., Chaudhry, Kauser and Cripps, Steve C. 2022. Mitigation of load mismatch effects using an orthogonal load modulated balanced amplifier. IEEE Transactions on Microwave Theory and Techniques 70 (6) , pp. 3329-3341. 10.1109/TMTT.2022.3167414

Publishers page: http://doi.org/10.1109/TMTT.2022.3167414

Please note:
Changes made as a result of publishing processes such as copy-editing, formatting and page numbers may not be reflected in this version. For the definitive version of this publication, please refer to the published source. You are advised to consult the publisher's version if you wish to cite this paper.

This version is being made available in accordance with publisher policies. See http://orca.cf.ac.uk/policies.html for usage policies. Copyright and moral rights for publications made available in ORCA are retained by the copyright holders.

Mitigation of Load Mismatch Effects Using an Orthogonal Load Modulated Balanced Amplifier

Roberto Quaglia, *Member, IEEE,* Jeffrey R. Powell, Kauser Chaudhry, and Steve C. Cripps, *Life Fellow, IEEE*

***Abstract*—This paper presents an orthogonal load modulated balanced amplifier designed to mitigate the effects of the load mismatch on the power added efficiency and output power of the amplifier. This is achieved by electronically adjusting the ratio between the two input signals of the power amplifier (in phase and amplitude) and the reactive termination at the output nominally isolated port. The mode of operation of the power amplifier is described using a theoretical analysis that highlights the role of the different tuning parameters, and is confirmed by simulations using a simplified transistor model. The design and characterization under load mismatch of a prototype power amplifier, working in the 1.6–3.2 GHz band are described and the experimental results compared to those of an analogous balanced power amplifier, where it is shown that the orthogonal balanced amplifier is able to increase substantially the mismatch region on which a given target performance is achieved.**

***Index Terms*—Antenna mismatch, balanced amplifier, gallium nitride, power amplifier, VSWR.**

I. Introduction

POWER amplifiers (PAs) for high-frequency applications are widely studied by the microwave community due to their impact on the fidelity and energy efficiency of wireless transmitters. While normally designed to operate on a nominal load equal to the system impedance ($50\,\Omega$ in most cases), the load presented to them during operation is unlikely to be $50\,\Omega$, with a Voltage Standing Wave Ratio (VSWR) larger than 1. The severity of the mismatch determines how much the PA performance changes compared to the nominal case, with some degradation for moderate VSWR, typical of mismatched antennas due to broadband operation or cross-talk in antenna arrays, and possible failures if the VSWR is very large, as for accidental disconnections of the load or high reflection due to object obstruction.

The consequences of PA load mismatch have been studied extensively. In [1] it was shown, with experimental data on a SiGe Heterojunction Bipolar Transistor (HBT) PA, that the effect of the mismatch was strongly related to the phase of the reflection coefficient presented to the PA, not only on the magnitude. This was later observed on a GaAs HBT as well [2]. The effect of mismatch in different class-E PA implementations was studied in detail in [3], while the works in [4]–[6] focused on the effect in Doherty PAs, and [7] on an envelope-tracked PA. In [8], [9], different PA architectures have been compared in terms of sensitivity to load mismatch, showing the advantage of using balanced PAs, which is the focus of the simplified study in [10]. In general, there is an agreement that load mismatch leads to degradation of output power, efficiency and linearity; this can be reflected in a change of behavioural model coefficients representing the PA [11] based on the load. Also, the study of circuit stability needs to account for the mismatch as well [12].

The most common way of avoiding mismatch affecting the PA behaviour is to use an isolator or circulator at the output of the PA. This helps to maintain the PA performance, but it cannot prevent a reduction of power delivery to the antenna and consequent reduction of the system efficiency, since the mechanism is simply to dissipate any reflected power into a load. Moreover, these non-reciprocal components are lossy, bulky and expensive, and avoiding them can have huge benefits for the cost of the whole system.

It does not come as a surprise that a great research effort is going into finding solutions to protect (from severe VSWR) or desensitize (from moderate VSWR) PAs from load mismatch without using isolators or circulators. To protect against failures with severe VSWR a number of approaches have been used [13]–[20]. For moderate VSWR, typical of mismatched antennas rather than accidental occurrences, the research effort is instead targeting the recovery of performance, or at least the mitigation of the degradation, in terms of output power, efficiency, and linearity. Considering that most PAs for telecom applications require linearization even on the nominal load, many papers have studied ways to make behavioral models [21]–[23] and digital predistorters [24]–[29] load dependent. To recover output power and efficiency, the retuning of the output matching network by controlling some electronically tunable components has been used [30]–[34], including with the use of MEMS [35] and metamaterials [36]. These solutions have to deal with the issue of inserting tunable elements directly in the path of the output signal, requiring those elements to handle high power signals and inevitably increasing the losses of the output matching network, as well as worsening distortion which is critical in some applications.

Efficiency enhancement PA techniques can also benefit from methods to reduce the effect of mismatch, and if designed properly can actually be used to compensate for mismatch. For example, dual-input Doherty PAs have shown the ability to compensate for moderate mismatch [37], [38]. Also, novel Doherty architectures such as a series/parallel [39], with balanced/Doherty configuration [40], or with DC supply adaptation [41], [42] can bring significant performance recovery compared to standard Doherty PAs. Also, properly designed

Manuscript received January 7, 2022; revised March 17, 2022; accepted April 9, 2022.

R. Quaglia, K. Chaudhry, S.C. Cripps are with the Centre for High Frequency Engineering, Cardiff University, Queens' Buildings, The Parade, CF24 3AA, Cardiff, UK e-mail: quagliar@cardiff.ac.uk

J.R. Powell is with Skyarna Ltd, Church Court, Halesowen, B63 3TT

and controlled outphasing PAs can be used in this context [43], while a Load Modulated Balanced Amplifier (LMBA) with low mismatch sensitivity was presented in [44].

In this paper, we propose a new method to improve the PA performance in the presence of load mismatch that is particularly suited for broadband PAs working in pulsed mode (e.g., for radar applications). The idea is to use an Orthogonal Load Modulated Balanced Amplifier (OLMBA) [45] architecture where the complex ratio between the main and Control Signal Power (CSP) inputs and the nominally isolated output port impedance can be controlled electronically to re-adapt the matching at the balanced devices and bring the device impedances closer to the optimum. This is a different approach compared to those presented in the papers discussed above since it can provide good RF bandwidth, and does not place any tunable component directly in the path of the output signal, hence relaxing the requirements in terms of losses and power handling. This paper also differs from previous work on LMBA [46]–[54] and OLMBA since it shows for the first time the ability to compensate for load mismatch using the OLMBA architecture.

The paper is organized as follows: Section II describes, with simplified models, the OLMBA mode of operation under load mismatch, and shows how tuning the parameters allows to bring the devices loads back near the optimum. Section III and IV describe the design and characterization of the prototype, respectively, with focus on the comparison with an analogous balanced PA, while Section V will draw some conclusions.

II. Mode of Operation

A. Theoretical analysis

The OLMBA schematic is represented in Fig. 1, where a balanced amplifier is modified by injecting a controlled CSP signal from the isolated input, and a reflective tunable load is connected to the isolated output. The CSP complex ratio to the main input is defined as α, while the isolated output is terminated with Γ_X. The analysis concerns the case where the output load is not terminated, generally $\Gamma_L \neq 0$.

For a simplified analysis, the transistors can be represented as current sources, assuming the coupler is ideal and directly connected to these sources, as in Fig. 2. The loaded output coupler can be reduced to a 2-port network whose impedance matrix is as follows:

$$\mathbf{Z} = Z_0 \begin{bmatrix} \frac{(1-\Gamma_L)(1+\Gamma_X)}{1+\Gamma_L\Gamma_X} & \frac{-j(\Gamma_L+\Gamma_X)}{1+\Gamma_L\Gamma_X} \\ \frac{-j(\Gamma_L+\Gamma_X)}{1+\Gamma_L\Gamma_X} & \frac{(1+\Gamma_L)(1-\Gamma_X)}{1+\Gamma_L\Gamma_X} \end{bmatrix} \tag{1}$$

where port 1 is the one directly connected to the load, and port 2 the one coupled to the load. Therefore, their currents are:

$$\begin{cases} I_1 = I_B(1-j\alpha) \\ I_2 = I_B(-j+\alpha) \end{cases} \tag{2}$$

where I_B is an arbitrary current, identical for the two devices, and α is the relative CSP value, as a complex quantity.

By multiplying the $\mathbf{Z}$ matrix of (1) with the currents of (2), we obtain the voltage at the two ports. By then dividing that

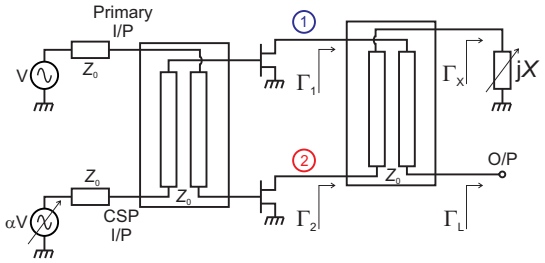

Fig. 1. OLMBA schematic.

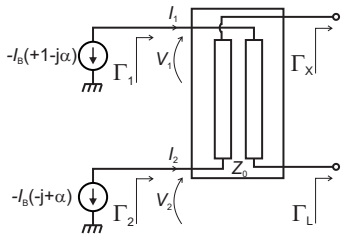

Fig. 2. OLMBA schematic for analysis.

by the respective currents, we can calculate the impedance normalized to Z_0 at the two ports:

$$\begin{cases} z_1 = \frac{1-\Gamma_L\Gamma_X}{1+\Gamma_L\Gamma_X} - 2\frac{\Gamma_L+j\alpha\Gamma_X}{(1+\Gamma_L\Gamma_X)(1-j\alpha)} \\ z_2 = \frac{1-\Gamma_L\Gamma_X}{1+\Gamma_L\Gamma_X} - 2\frac{\alpha\Gamma_X+j\Gamma_L}{(1+\Gamma_L\Gamma_X)(\alpha-j)} \end{cases} \tag{3}$$

We can then calculate the reflection coefficient at the two ports, which results in:

$$\begin{cases} \Gamma_1 = \frac{-\Gamma_L(1+\Gamma_X)-j\alpha\Gamma_X(1-\Gamma_L)}{1-\Gamma_L-j\alpha(1+\Gamma_X)} \\ \Gamma_2 = \frac{+\Gamma_L(1-\Gamma_X)-j\alpha\Gamma_X(1+\Gamma_L)}{1+\Gamma_L+j\alpha(1-\Gamma_X)} \end{cases} \tag{4}$$

Equation (4) shows a rather non-trivial relationship between the impedance at ports (Γ_1, Γ_2, Γ_L) and the design parameters Γ_X and α. Let's analyse the effect of each separately.

B. Balanced case

The balanced amplifier case is found by imposing terminated isolated ports at the output ($\Gamma_X = 0$) and input ($\alpha = 0$). Therefore, the reflection coefficients are:

$$\begin{cases} \Gamma_1 = \frac{-\Gamma_L}{1-\Gamma_L} \\ \Gamma_2 = \frac{\Gamma_L}{1+\Gamma_L} \end{cases} \tag{5}$$

which, for $\Gamma_L \ll 1$ are:

$$\begin{cases} \Gamma_1 \simeq -\Gamma_L \\ \Gamma_2 \simeq +\Gamma_L \end{cases} \tag{6}$$

The load presented at the two devices is symmetric with respect to the centre of the Smith Chart, meaning that the two active devices will both be mismatched, but in "opposite directions", leading to the intrinsic robustness of balanced PAs to load mismatch. It is important to note, however, that once Γ_L starts being substantial, the symmetry is lost (see

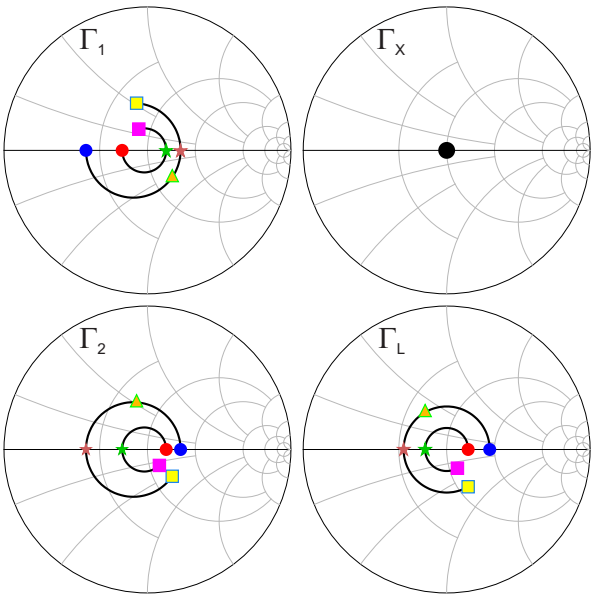

Fig. 3. Reflection coefficient at balanced PA ports (Γ_1, Γ_2) under load mismatch (Γ_L).The output isolated port is teminated ($\Gamma_\mathrm{X}=0$).

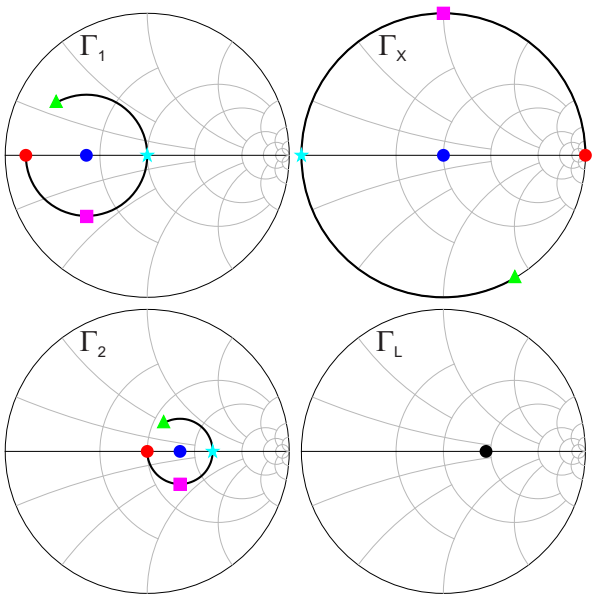

Fig. 4. Reflection coefficient at balanced PA ports (Γ_1, Γ_2) with $\Gamma_\mathrm{L}=0.3$, with swept χ.

Fig. 3). While the inner mismatch circle on Γ_L shows a good symmetry once translated to the Γ_1, Γ_2 planes, the outer circle leads to a marked asymmetry and a larger deviation from $|\Gamma_\mathrm{L}|$.

Moreover, if the devices are driven close to saturation, one of the devices will go potentially into hard clipping, invalidating the current source assumption. Therefore, the resilience of balanced PAs can be explained only for small mismatch, by approximating the transistors as current sources.

Another important observation can be made after calculating the power at the output (P_L) and output isolated (P_X) ports. Their ratio can be written as:

$$\frac{P_\mathrm{X}}{P_\mathrm{L}}=\frac{|\Gamma_\mathrm{L}|^2}{1-|\Gamma_\mathrm{L}|^2} \tag{7}$$

meaning that a greater amount of RF power is dissipated in the isolated load as the mismatch worsens. Here we observe that the total power generated by the devices is not affected by Γ_L if they stay linear. They continue to generate the same power, but only a portion of that reaches the output load. Therefore, the resilience of the balanced PA to mismatch in terms of maintaining an acceptable matching at each device still comes with a cost in terms of output power and efficiency. For example, a VSWR of 2 leads to 12.5% of the output power being dissipated in the isolation load, while with VSWR of 3 that portion rises to 33%.

C. Effect of Γ_X- Terminated CSP I/P Port

From the analysis of the balanced case, it is clear that the mismatch introduces an unbalancing of the balanced devices. In the balanced case, the "imbalanced" power is redirected to the terminated isolated port by the coupler. In the OLMBA, the matched termination is substituted by a generic Γ_X which will be assumed as reactive ($|\Gamma_\mathrm{X}|=1$, $\Gamma_\mathrm{X}=\mathrm{e}^{j\chi}$) so that no RF power is dissipated at that port. For the OLMBA to show any advantage over the standard balanced PA, it is necessary to show that it can also mitigate the mismatch at the ports. Let's start from the case with $\alpha=0$. The reflection coefficients result as:

$$\begin{cases}\Gamma_1=\frac{-\Gamma_\mathrm{L}(1+\Gamma_\mathrm{X})}{1-\Gamma_\mathrm{L}}=\frac{-\Gamma_\mathrm{L}(1+\mathrm{e}^{j\chi})}{1-\Gamma_\mathrm{L}}\\ \Gamma_2=\frac{+\Gamma_\mathrm{L}(1-\Gamma_\mathrm{X})}{1+\Gamma_\mathrm{L}}=\frac{+\Gamma_\mathrm{L}(1-\mathrm{e}^{j\chi})}{1+\Gamma_\mathrm{L}}\end{cases} \tag{8}$$

Compared to the balanced case (5), the Γ_X amplifies the two reflection coefficients by two different factors. Some notable cases are for $\chi=0$ (open circuit), that leads to $\Gamma_2=0$, meaning that the device coupled with the output is "immunized" to load variation, but that also magnifies $|\Gamma_1|$, and for $\chi=\pi$ (short circuit) which puts $\Gamma_1=0$ but maximizes $|\Gamma_2|$. The case for $\Gamma_\mathrm{X}=\pm j$, which corresponds to an isolated termination of $\pm jZ_0$, leads to the same "amplification" in $|\Gamma_1|$ and $|\Gamma_2|$. Fig. 4 and Fig. 5 show the effect of Γ_X for two cases of Γ_L.

However, in general, the adjustment of χ alone does not seem to give enough degrees of freedom to bring the loads at the devices' port to a more favourable condition.

D. Effect of CSP

With $\Gamma_\mathrm{X}=0$, i.e. a balanced amplifier with a control signal injected at the normally isolated input port, the equations in (4) become:

$$\begin{cases}\Gamma_1=\frac{-\Gamma_\mathrm{L}}{1-\Gamma_\mathrm{L}-j\alpha}\\ \Gamma_2=\frac{+\Gamma_\mathrm{L}}{1+\Gamma_\mathrm{L}+j\alpha}\end{cases} \tag{9}$$

While it would seem that selecting a sufficiently large $|\alpha|$ would reduce the mismatch, in reality it means that the all the power would be dissipated in the isolated port, which is clearly not a good solution.

On the other hand, when applying a CSP signal together with a reflective Γ_X, i.e. by using the full equations from (4),

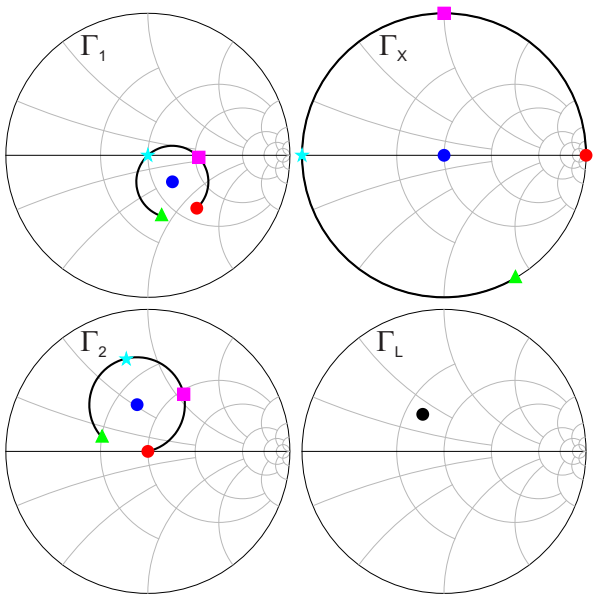

Fig. 5. Reflection coefficient at balanced PA ports (Γ_1, Γ_2) with e^{j120°, with swept χ.

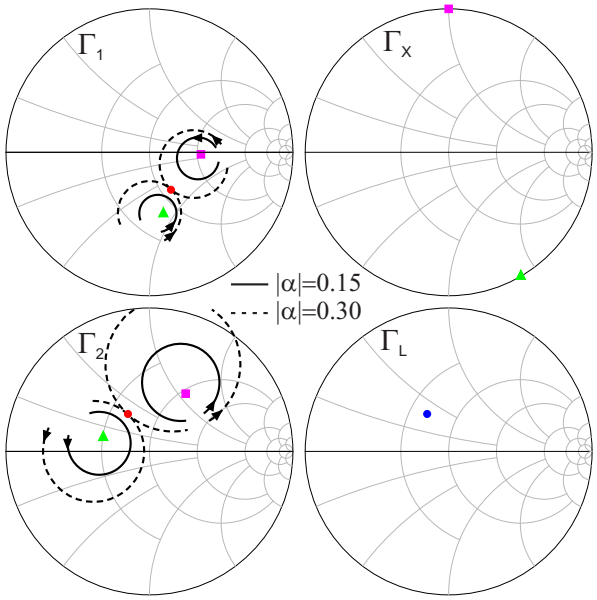

Fig. 6. Reflection coefficient at balanced PA ports (Γ_1, Γ_2) with $\Gamma_L = 0.3e^{j120^\circ}$, for $\chi = 90^\circ$ (magenta square) and 210° (green triangle). The phase of α is swept from 0 to 330° (direction of the arrow), while the amplitude is 0.15 (solid black line) and 0.3 (dashed black line). The red circles highlight the case $\alpha = j\Gamma_L$ that leads to $\Gamma_2 = -\Gamma_1 = \Gamma_L$.

it can be noticed how, by varying the complex value α, the two reflection coefficients move on circles, as the phase of α sweeps around the point fixed by Γ_L and Γ_X, see Fig. 6.

E. Notable cases

There are two particular cases of parameters' settings worth highlighting.

Firstly, the case of $\Gamma_2 = -\Gamma_1 = \Gamma_L$, which represents an outcome similar, but considerably improved, to a regular balanced amplifier having the same mismatched load; inasmuch as the device plane reflection magnitudes remain the same as $|\Gamma_L|$ regardless of the magnitude and phase of Γ_L. This condition can be analysed as follows, again using (4) :

$$\begin{cases} -\Gamma_1 = \Gamma_L = \frac{+\Gamma_L(1+e^{j\chi})+j\alpha e^{j\chi}(1-\Gamma_L)}{1-\Gamma_L-j\alpha(1+e^{j\chi})} \\ +\Gamma_2 = \Gamma_L = \frac{+\Gamma_L(1-e^{j\chi})-j\alpha e^{j\chi}(1+\Gamma_L)}{1+\Gamma_L+j\alpha(1-e^{j\chi})} \end{cases} \tag{10}$$

Expanding either of these equations leads to the same result:

$$j\alpha(e^{j\chi}+\Gamma_L) = -\Gamma_L(e^{j\chi}+\Gamma_L) \tag{11}$$

that gives the values of the CSP drive, α, as

$$\alpha = j\Gamma_L \tag{12}$$

which will apply for any value of χ, a truly remarkable result meaning that the OLMBA can be used, by CSP action only, to bring the impedance at the devices to the same condition as the balanced PA, *but without dissipating RF power at the isolated port*. In comparison with the matched case, there is a decrease in output power as $1-|\Gamma_L|^2$. This is the same as the balanced case, where for example for a $|\Gamma_L| = 0.25$, the output power is still 94% of the matched case. For this OLMBA configuration, however, the output power corresponds to the total power generated by the devices, potentially improving the efficiency of the system compared to the balanced case. This OLMBA case is highlighted in Fig. 6 with the red circle symbols at the intersection of the dashed trajectories.

A second noteworthy case, the condition $\Gamma_1 = \Gamma_2$, which reveals a specific value for the two device plane impedance which can be realized by suitable settings of α and χ.

The equations in (4) can be re-organized to highlight the common terms for the two reflection coefficients:

$$\begin{cases} \Gamma_1 = 1-(1+\Gamma_L e^{j\chi})\frac{1-j\alpha}{1-\Gamma_L-j\alpha(1+e^{j\chi})} \\ \Gamma_2 = 1-(1+\Gamma_L e^{j\chi})\frac{1+j\alpha}{1+\Gamma_L+j\alpha(1-e^{j\chi})} \end{cases} \tag{13}$$

Therefore, to obtain $\Gamma_1 = \Gamma_2$ we equate the second part of the equations:

$$\frac{1-j\alpha}{1-\Gamma_L-j\alpha(1+e^{j\chi})} = \frac{1+j\alpha}{1+\Gamma_L+j\alpha(1-e^{j\chi})} \tag{14}$$

leading to the identity:

$$\Gamma_L = \alpha^2 e^{j\chi} \tag{15}$$

meaning that we need to set the following conditions for impedance tracking at the two ports:

$$\begin{cases} |\alpha| = \sqrt{|\Gamma_L|} \\ \angle\alpha = \frac{1}{2}(\angle\Gamma_L - \chi) \end{cases} \tag{16}$$

The resulting reflection coefficient at the ports is:

$$\Gamma_1 = \Gamma_2 = -j\alpha\, e^{j\chi} = -j\sqrt{\Gamma_L e^{j\chi}} \tag{17}$$

This condition is potentially useful inasmuch as it shows that for any magnitude of the mismatched termination Γ_L, there exists a value of α and Γ_X which brings each device termination to a single point. On the other hand, the reflection coefficient obtained is larger in magnitude than the one presented at the output.

F. Pre-matching

The effect of pre-matching networks between the coupler ports and the intrinsic generator planes can be studied analytically if the pre-matching networks are assumed identical and loss-less on the two ports, and provide a perfect transformation between Z_0 and the optimum load of the transistor $R_{\rm opt}$. In this scenario, accounting for a phase delay $-\theta$ introduced by these networks, the cascade coupler + pre-matching networks can be seen as an equivalent coupler with the following Z-matrix:

$$\mathbf{Z} = R_{\rm opt} \begin{bmatrix} \frac{(e^{j2\theta}-\Gamma_{\rm L})(e^{j2\theta}+\Gamma_{\rm X})}{(e^{j4\theta}+\Gamma_{\rm L}\Gamma_{\rm X})} & \frac{-j(\Gamma_{\rm L}+\Gamma_{\rm X})e^{j2\theta}}{(e^{j4\theta}+\Gamma_{\rm L}\Gamma_{\rm X})} \\ \frac{-j(\Gamma_{\rm L}+\Gamma_{\rm X})e^{j2\theta}}{(e^{j4\theta}+\Gamma_{\rm L}\Gamma_{\rm X})} & \frac{(1+\Gamma_{\rm L})(e^{j2\theta}-\Gamma_{\rm X})}{(e^{j2\theta}+\Gamma_{\rm L}\Gamma_{\rm X})} \end{bmatrix} \quad (18)$$

The reflection coefficients at the ports, now referenced to $R_{\rm opt}$ become:

$$\begin{cases} \Gamma_1 = e^{-j2\theta}\frac{-\Gamma_{\rm L}(e^{j2\theta}+\Gamma_{\rm X})-j\alpha\Gamma_{\rm X}(e^{j2\theta}-\Gamma_{\rm L})}{[e^{j2\theta}-\Gamma_{\rm L}-j\alpha(e^{j2\theta}+\Gamma_{\rm X})]} \\ \Gamma_2 = e^{-j2\theta}\frac{+\Gamma_{\rm L}(e^{j2\theta}-\Gamma_{\rm X})-j\alpha\Gamma_{\rm X}(e^{j2\theta}+\Gamma_{\rm L})}{[e^{j2\theta}+\Gamma_{\rm L}+j\alpha(e^{j2\theta}-\Gamma_{\rm X})]} \end{cases} \quad (19)$$

It can be shown that the pre-matching does not have an effect on the tuning capabilities, but only changes the phase settings for $\Gamma_{\rm X}$ and α to achieve the same reflection coefficient. For example, the first notable case in II-E can be now described as $\Gamma_2 = -\Gamma_1 = \Gamma_{\rm L}e^{-j2\theta}$ by setting:

$$\alpha = j\Gamma_{\rm L}e^{-j2\theta} \quad (20)$$

leading to the same advantages compared to balanced PA as discussed in II-E.

III. Prototype design

The two special cases discussed in II-E are clearly interesting and tell us that the adjustment of the tunable parameters α and χ leads to an effective re-adjustment of the device impedances. They do not, however, in general represent optimum solutions for obtaining maximum power and/or efficiency when considering real devices with limited gain and saturation effects, as well as real networks and couplers. The latter is particularly relevant since the OLMBA has proven to be able to boost the PA performance beyond the bandwidth of the 3 dB quadrature coupler [45], where the analysis in the mismatch case is too complex.

As such, the remainder of this paper will focus on a prototype design simulated using the large signal model of the device. The tuning parameters will be swept over their full range to evaluate the potential of the technique when considering the global performance, rather than the device plane impedance only.

The OLMBA circuit described in this paper uses a computer aided design method which determines the adaptive control parameters for peak circuit operation as the printed circuit board designs are evolved. Conventional amplifier design strategies use a variety of circuit synthesis and optimisation approaches to present the transistors with optimal impedance at fundamental and in many cases harmonic frequencies; although harmonic tuning is almost always limited to amplifiers

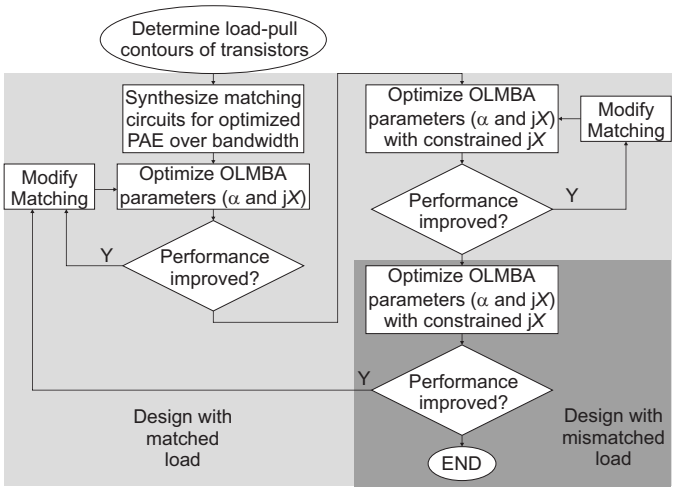

Fig. 7. Design flow for OLMBA with load mismatch resilience.

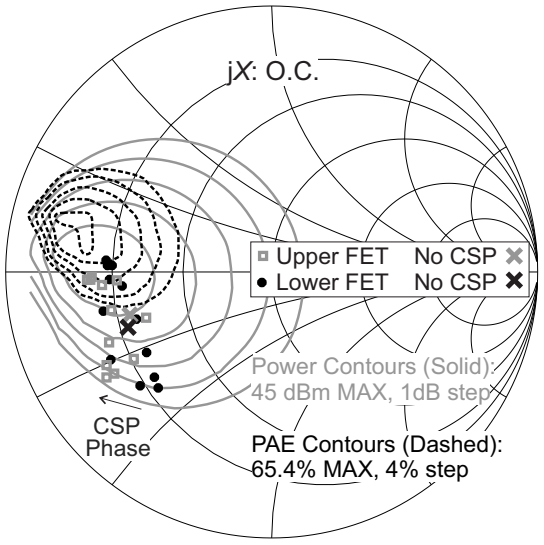

Fig. 8. Simulated impedance at the OLMBA transistors current generator planes as α phase is swept over 360° for CSP power -6dB below input power, and $\Gamma_{\rm X}$ open circuit. Frequency: 2800 MHz. Data also plotted for no CSP applied. Power and PAE contours are plotted.

with modest bandwidth, typically $< 20\%$. Broadband harmonic control via harmonic injection has been demonstrated in literature [55], but it has not been considered for this first prototype.

Many design approaches derive from the Cripps method [56], where matching circuit performance can be compared to computed, or measured, power/efficiency contours using small signal analysis of the matching circuits. Employing adaptive control, as described here for the OLMBA, provides for the impedance presented to the transistors to be perturbed using the control signal. As noted, this adaptive property of the OLMBA makes it particularly well suited to improved performance over extended bandwidth and in load mismatch conditions. Since dynamic parameter adjustment will be used in the eventual hardware, matching circuit synthesis can be performed using circuit optimisation and iterative layout improvement in the following way (see Fig. 7):

A. Design Method

- Matching circuits are synthesised to optimise PAE over the target bandwidth based on transistor load-pull data.
- This circuit is simulated using a circuit optimiser (random followed by gradient in this case) to continuously adjust α phase and magnitude (constrained to -10 dB to -6 dB relative to Pin) and Γ_{X} phase,χ, ($|\Gamma_{\mathrm{X}}| = 1$).
- If the circuit performance is improved under optimisation compared to the previous adaptively controlled amplifier layout, impedance trajectories under adaptive control can be compared to the transistor load-pull in order to use the matching networks to reposition the impedance for optimal adaptive performance advantage over the design bandwidth. Fig. 8 illustrates how the adaptive control modifies the device impedance at 2.8 GHz, for example. In the figure the impedance at each transistor is plotted as α phase is swept through $360°$, for a CSP power 6 dB below the input power, and Γ_{X} open circuit. Compared to the no CSP position (the native matching circuit response) phases of α can be chosen which place the FET impedance more favourably with respect to the device load-pull contours plotted.
- When no further improvement is possible, the optimised Γ_{X} phases are examined and translated into achievable discrete values. In this demonstrator circuit a SP4T switch is used to configure Γ_{X}. Fig. 10 shows the final Γ_{X} states selected after completing all design steps.
- Further optimisation of the matching circuit and component values are performed until no improvement is observed.
- Finally, the design, which has been completed for an amplifier "seeing" a matched load, is now simulated into the required mismatch load conditions. Where performance improvement can be attained using matching circuit optimisation, further circuit design iteration can be undertaken.

In practice the design process described above and in Fig. 7 lends itself to an automated nested design process – in particular considerable databases for control parameters are generated where wide bandwidth and large load impedances ranges are required. It is anticipated that a global performance metric can be used to drive this entire design loop, such as the Smith Chart area coverage discussed below (Fig. 24). Although this could, in principle, be implemented automatically using a nested optimisation as described, the first demonstrator was designed using manual intervention for the matching network layouts and also the Γ_{X} component choices; based on examination of the impedance data such as Fig. 8.

B. Design Implementation

Fig. 9 shows the full circuit schematic of the OLMBA circuit, with microstrip transmission line dimensions shown in mm. Two 25W GaN transistors from Wolfspeed (CGH40025F-ND) together with surface mount Xinger couplers (11306-3S) were used in balanced and OLMBA circuits. The circuits were fabricated on Rogers RO4350 0.508 mm thick substrates which were attached to machined aluminium carriers. The balanced

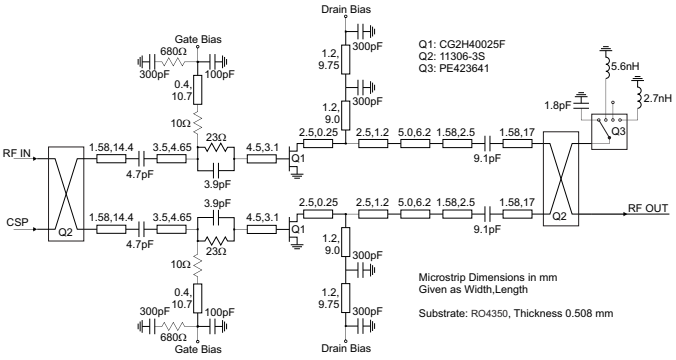

Fig. 9. Schematic of the OLMBA prototype. Electrical length of transmission lines are calculated at 2.4 GHz.

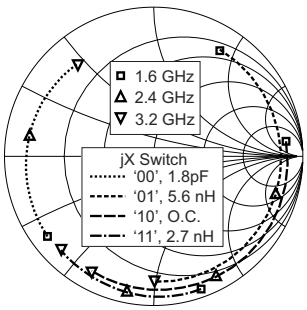

Fig. 10. Simulated reflection coefficient at the input of the jX switch vs. frequency, at different switch settings selecting different loads.

PA is identical, except for the jX switch being removed and substituted by 4x200 Ω SMD resistors in a 0805 package to provide a 50 Ω termination with sufficient power handling. Also, the CSP input is terminated with an external 50 Ω SMA termination.

Unconditional circuit stability was achieved using damping resistors in the gate bias lines, and also parallel RC sections in the input circuit. The input circuit was further optimised to maximise gain and therefore PAE. Stepped impedance transformers were used in the output matching circuit, as these were found to allow adjustment of the transistor impedance over extended bandwidth according to the method described above.

For the OLMBA a SP4T digitally controlled switch from Peregrine Semiconductor (PE423641) was used. The datasheet maximum input power rating for this part is 37 dBm for matched ports. OLMBA circuit simulations showed incident powers above this level under extreme mismatch conditions. Testing of standalone switches were performed to determine the switch compression characteristics for reactively terminated switch ports (as for the OLMBA circuit) and at raised power levels, and no failures were observed up to input power levels of 40 dBm. In practice, several OLMBA circuits have been tested for more than 100 hours under a variety of amplifier mismatch and jX setting, with no switch failures under RF pulsed conditions in deep class AB, suggesting that this solution is robust for this type of application and power levels. For the circuit simulations small signal s-parameter data for the switch and lumped components forming jX were used to estimate the values for Γ_{X} for each switch condition. Fig. 10

plots the simulated reflection coefficient for each of the 4-switch states that were employed.

C. Simulation results

The simulation of the OLMBA has been performed by sweeping different variables:

- RF frequency: from 1600 to 3200 MHz with a 200 MHz step.
- 144 Γ_{L} points within a maximum magnitude of 0.6.
- Switch control, on 4 values indicated as '00', '01', '10', '11', and corresponding to nominal loads of 1.8 pF, 5.6 nH, Open Circuit, and 2.7 nH, respectively.
- Relative amplitude of the CSP signal, with no CSP, at -10 dB and -6 dB.
- Relative phase of the CSP signal, with 30 degree steps.
- RF input drive, up to 3 dB compression (maximum drive established at the $\Gamma_{\mathrm{L}} = 0$ condition).

For the balanced amplifier, the same approach has been followed without the sweeps on the CSP and switch conditions.

This type of simulation generates a vast database which is difficult to visualize in a compact way. Therefore, a choice was made to use as a representative measurement the point at which the maximum PAE is achieved, at each frequency and load, when sweeping all variables. The PAE, output power and gain at this condition are then used to plot Γ_{L} contours at each frequency, allowing an easier assessment of the advantages introduced by the OLMBA compared to the balanced power amplifier.

In our opinion, using the maximum PAE point provides a fairer comparison between OLMBA and balanced, since the OLMBA is a dual input amplifier, the PAE intrinsically accounts for the extra power used by the OLMBA at the input. At the same time, plotting the output power contours associated with the maximum PAE points enables us to determine if the output power degradation has become too excessive or unacceptable. Comparison at same input drive level would be another option, but it would raise questions about what input (single-ended or combined) shall we use for the OLMBA. The final result on the comparison would not change, however this could raise questions about the choice or suitability of the input signal (single-ended vs combined) for the OLMBA. The final outcome of the comparative analysis does not change, with the OLMBA still providing better resilience.

Fig. 11 shows the simulated PAE contours obtained with this method for different jX switch conditions at 2.8 GHz, therefore already corresponding to the best CSP settings leading to maximum PAE for each load. The grey thin contours are equally spaced between the minimum and maximum recorded PAE values, while the black thick contours are fixed at 45% PAE, selected as a reference value. It is worth noticing how the PAE contours move around the Smith Chart for different jX settings, demonstrating the reconfigurability of the OLMBA. Fig. 12 merges the contours of Fig. 11 and compares these to those of the balanced PA, showing that by exploiting the OLMBA parameters' tuning, the performance of the PA can be maintained over a larger mismatch, corresponding to a larger Smith Chart area coverage of contours. It must be noted

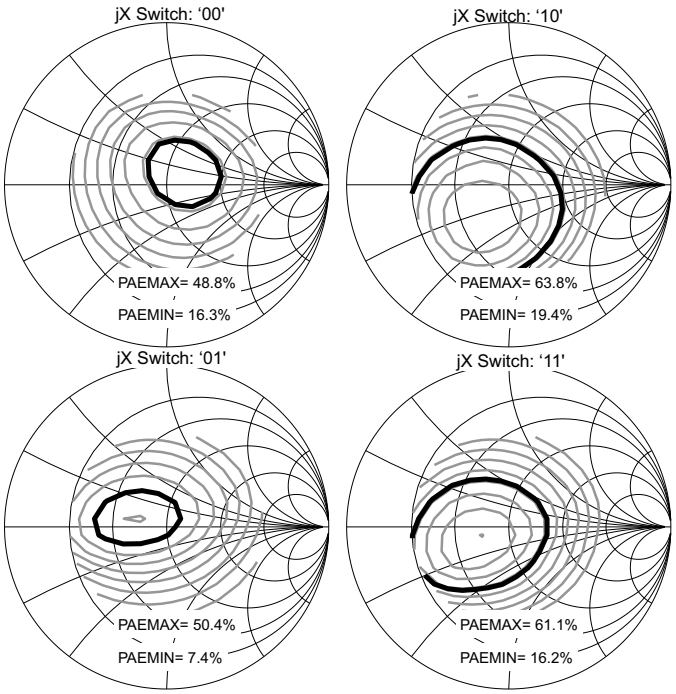

Fig. 11. Simulated PAE contours for OLMBA considering the best PAE condition for the CSP settings, at 2.8 GHz. The jX switch is set at different states in each plot. The 45% PAE contour is highlighted in black.

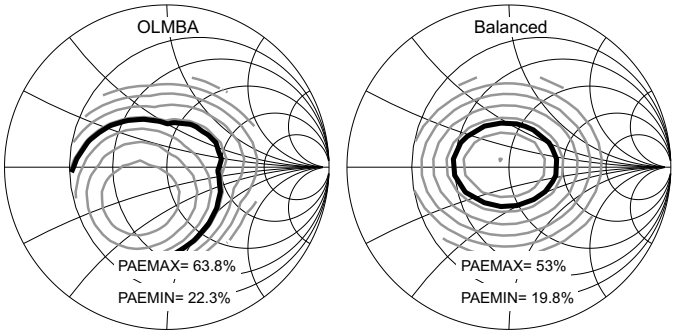

Fig. 12. Simulated PAE contours for OLMBA considering the best PAE condition for the CSP and jX switch settings (left), and balanced PA (right), at 2.8 GHz. The 45% PAE contour is highlighted in black.

that the absolute maximum PAE value for the OLMBA is higher than that of the balanced PA, but not in the matched case (50 Ohm) where the balanced PA compares fairly to the OLMBA. Load mismatch can in fact lead to a condition where, after OLMBA action both devices are terminated with loads closer to the optimum for PAE rather than for output power, thus improving the overall PAE.

By calculating the Smith Chart area coverage for PAE larger than a given target at each simulation frequency, it is possible to plot the graphs of Fig. 13, which again compare OLMBA and balanced PA and demonstrate the better performance of the former against load mismatch.

The circuits have been fabricated on RO4350 microstrip substrate with 0.508 mm dielectric thickness, and mounted on an aluminium carrier with panel mount SMA launchers for the RF ports. The pictures of the prototypes are shown in Fig. 14.

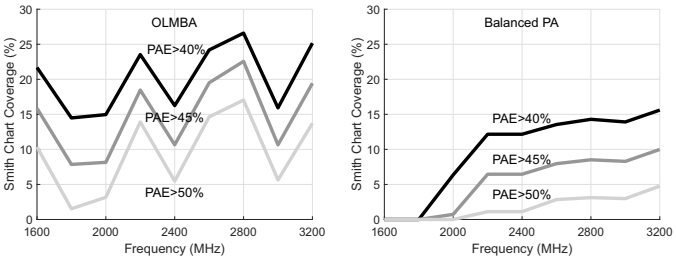

Fig. 13. Comparison OLMBA (left) vs. balanced PA (right) in terms of the Smith Chart area coverage for maximum PAE higher than a target, vs. simulation frequency.

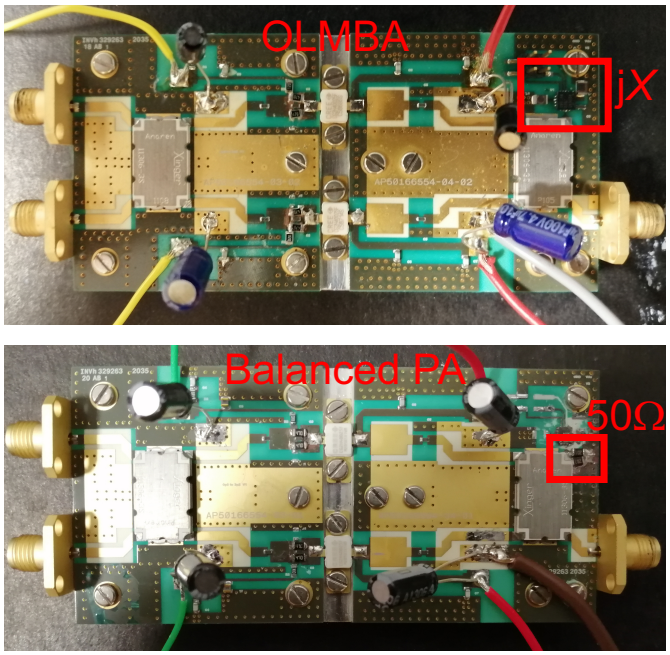

Fig. 14. Picture of OLMBA (top) and balanced PA (bottom) prototypes.

IV. Experimental Characterization

A. Measurement method

The characterization setup (Fig. 15) is based on a dual-output RF generator, the MG3710A by Anritsu. Channel 1 is used as principal RF input, while channel 2 is used for the CSP generation. By sharing the local oscillator, the relative phase between the two channels is maintained in the long term and also when moving back to the same frequency from a different setting. This is very important to ensure that a certain CSP condition can be tested repeatedly. The two RF channels are amplified by similar power amplifier drivers. A mechanical impedance tuner (CCMT-708) from Focus Microwave is used to tune Γ_L and controlled by the FDCS® software from Focus Microwave. The whole system is controlled by a computer using a Matlab® code.

The ratio of available input power between principal and CSP inputs is kept within 0.2 dB of the nominal setting at the DUT ports by measuring the input incident and reflected power through dual-directional couplers.

The relative phase is set at the generator plane for sweeping purposes. However, the relative phase at the DUT plane can

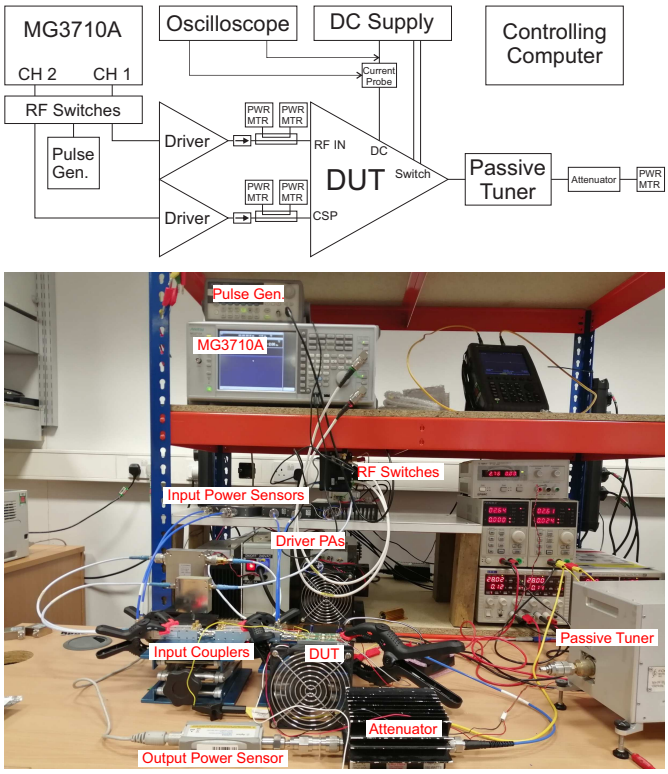

Fig. 15. Block Diagram and labelled picture of the characterization setup.

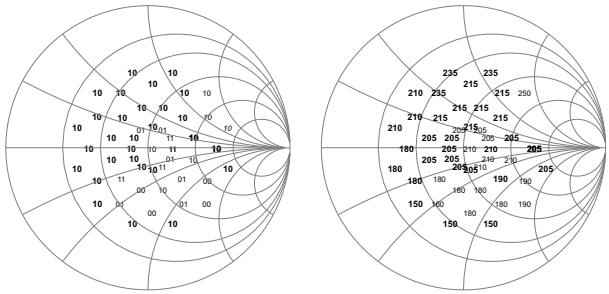

Fig. 16. Look-up table of the settings to optimize maximum PAE in the measured OLMBA at 2.6 GHz. Switch condition: left. CSP phase at the DUT ports: right. The relative CSP power is indicated by the font. No CSP: small font, italic (for left plot only). CSP at -10dB: small font, plain. CSP at -6 dB: large font, bold.

be calibrated after the measurements are taken. This is done by applying the same input power and CSP (amplitude and phase) sweeps on a hybrid coupler with known 4-port s-parameters. The relative phase at the DUT reference planes can be calibrated by identifying the phase settings at which the output power of the coupler reaches a minimum, and comparing it with the value expected from the coupler s-parameters. The prototypes have been measured in a realistic condition for radar applications, with a single tone input pulsed at 10% duty cycle, pulse duration of $1\mu s$. The key measurements are the output power, the gain, and the PAE. The gain and PAE are calculated using the total input power, that in the case of the OLMBA is the sum of the available power at the principal and CSP RF inputs.

An oscilloscope with current probe is used for the measure-

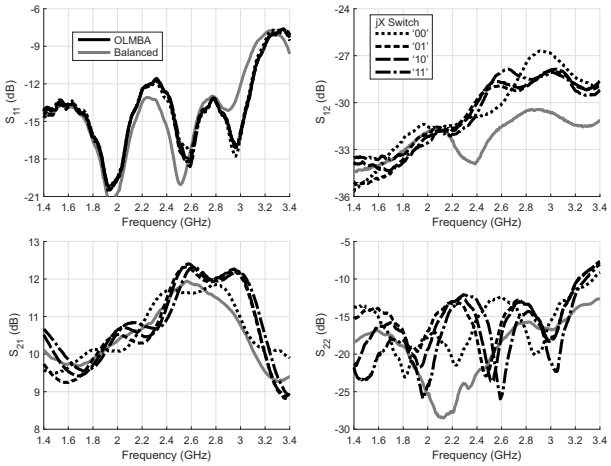

Fig. 17. Measured scattering parameters for the balanced PA and OLMBA at different switch conditions. Drain bias: 28 V, 50 mA per device.

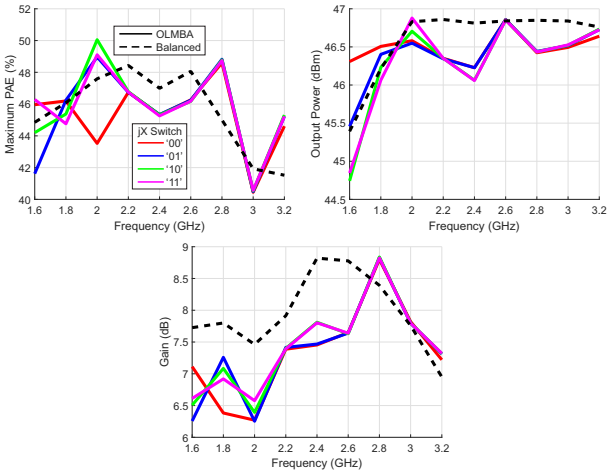

Fig. 18. Comparison between OLMBA and balanced prototypes. Maximum PAE, associate output power and gain vs. measurement frequency, on $\Gamma_{\mathrm{L}} = 0$. Gain compression of 3 dB.

ment of the drain voltage and current over the RF pulse, while wideband power sensors are used for the RF power readings.

The characterization of the OLMBA has been performed by sweeping different variables:

- RF frequency: from 1600 to 3200 MHz with a 200 MHz step.
- $|\Gamma_{\mathrm{L}}|$, with values 0, 0.15, 0.3, 0.45, 0.55.
- $\angle\Gamma_{\mathrm{L}}$, with 30° steps and starting point staggered by 15° at successive magnitude values.
- Switch control, on 4 values indicated as '00', '01', '10', '11', and corresponding to nominal loads of 1.8 pF, 5.6 nH, Open Circuit, and 2.7 nH, respectively.
- Relative amplitude of the CSP signal, with no CSP, at -10 dB and -6 dB (the latter only on the 2200–3200 MHz range).
- Relative phase of the CSP signal (compared to the input signal), with 30 degree steps.
- RF input drive, up to 3 dB compression (maximum drive established at the $\Gamma_{\mathrm{L}} = 0$ condition).

For the balanced amplifier, the same approach has been followed without the sweeps on the CSP and switch conditions.

The same method used for simulations for selecting the plot points have been used here, targeting mainly the maximum PAE points. At each frequency it is possible to generate a look-up table of the CSP and switch settings that maximize the target performance at each load. As an example, Fig. 16 show the optimum settings for the measured OLMBA at 2.6 GHz.

B. Results on 50 Ohm load

The first set of measurements is performed without load mismatch and zero CSP power to provide a performance benchmark, as well as making sure that the balanced PA is in fact comparable to the OLMBA in nominal conditions. The small signal scattering parameters (results in Fig. 17) for both amplifiers have been measured on the 1.4-3.4 GHz range, at the drian bias point of 28 V and 50 mA per device. This bias condition is maintained for all the characterisation campaign. As expected, the two amplifiers behave very similarly, with the change in jX switch condition having a minor effect for the OLMBA. Fig. 18 shows the results vs. frequency extracted from the power sweeps, selecting the maximum PAE point and the corresponding output power and gain. It can be noticed how the balanced PA has very similar performance to the OLMBA, except for the low frequency points where the quadrature coupler used rolls off (being defined for 2-4 GHz operation) and the OLMBA can give advantages in terms of output power performance. While the authors acknowledge that further circuit optimisation whilst taking into account mismatch might be considered to yield improved results for the balanced amplifier, this measurement shows that the balanced PA used here allows for at least a fair comparison having the equivalent baseline performance into 50 Ω.

C. Results with mismatched load

Fig. 19 to Fig. 21 report the maximum PAE contours together with the corresponding output power and gain contours, comparing OLMBA (top row) and balanced PA (bottom row) at the measurement frequencies. The grey thin contours use a 5% step for PAE, and 0.5 dB for output power and gain. The black thick contours have been set arbitrarily at 45% for PAE, 44 dBm for output power (corresponding to the power of at least one device in the balanced pair), and 7 dB for gain (which is around 3 dB compression from the small signal gain at centre band).

For a clearer explanation of how the contours have been generated, Fig. 23 shows the results of the OLMBA measurements at 3 GHz on $\Gamma_{\mathrm{L}} = 0.3^{\angle 195^\circ}$, highlighting the maximum PAE point used for constructing the contours of PAE, output power and gain. The results show that, in this particular case, the CSP action allows improvement in output power and PAE significantly if the CSP magnitude and phase are selected properly. It is worth noticing that increasing CSP power is not always providing a performance enhancement, with the -10 dB setting improving all metrics, while the -6 dB settings leading to gain and output power reduction. In this particular case, it is also interesting to note that the jX switch settings

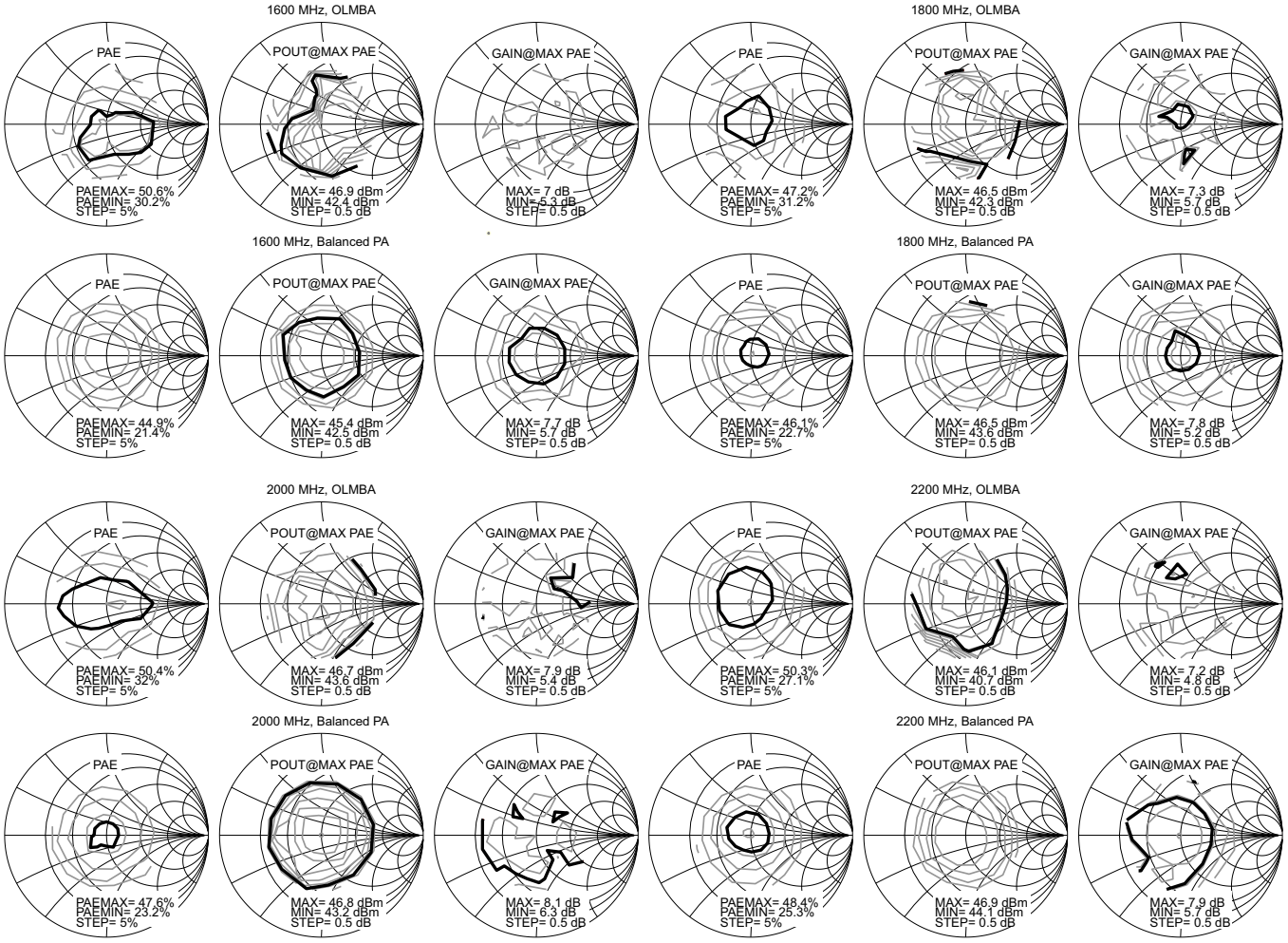

Fig. 19. OLMBA and balanced PA contours from 1600 to 2200 MHz, evaluated at maximum PAE point. Black thick contours highlight PAE of 45%, output power of 44 dBm, and gain of 7 dB. Grey thin contours limits and steps indicated in the legends.

only provide a small change of performance. Fig. 22 shows the same plot at 1.6 GHz on $\Gamma_{\mathrm{L}} = 0.15^{\angle 30^\circ}$.

At this frequency, the jX switch plays a much more important role due to the unbalancing of the coupler.

The extensive data display generated allows one to appreciate the advantages of the OLMBA approach over the whole frequency octave. The first thing to notice is that, at all frequencies, the OLMBA offers a better PAE vs. mismatch. Taking the 45% PAE contours as a reference, their area is always larger for OLMBA than for the balanced PA. The improvement is maximum at the ends of the band, but it is still significant at centre frequency. Importantly, the improvement in the PAE vs. mismatch is always accompanied by an improvement, or at least minimal degradation, of the corresponding output power, meaning that the OLMBA is not just trading PAE for output power. On the other hand, since the PAE improvement is achieved by means of CSP action, some decrease of gain is expected as confirmed by the gain contours. On average, a gain decrease of 0.7 dB is observed in the OLMBA compared to the balanced PA, except at the highest frequencies where the OLMBA offers also better gain. The gain contours are also the least uniform for the OLMBA case, due to the discrete variation of CSP levels across the tested load conditions. In a practical implementation, this might require some form of input equalization. Alternatively, the same experiment and contour creation can be repeated at fixed input power.

By analogy to the simulated plot in Fig. 13, Fig. 24 summarizes the comparison for the maximum PAE case by comparing the Smith Chart coverage at different levels of PAE, plotted vs. frequency.

A similar summary plot can be generated by observing a completely different subset of data. Fig. 25, for example, shows the Smith Chart coverage in terms of maximum output power, when selecting the maximum output power point for both the OLMBA and balanced PA (instead of the maximum PAE point). As for maximum PAE, the maximum output power shows that the OLMBA offers better mismatch resilience than the balanced PA.

V. Conclusion

The orthogonal load modulated balanced amplifier (OLMBA) proposed in this paper is capable of mitigating significantly the effects of load mismatch in a power amplifier.

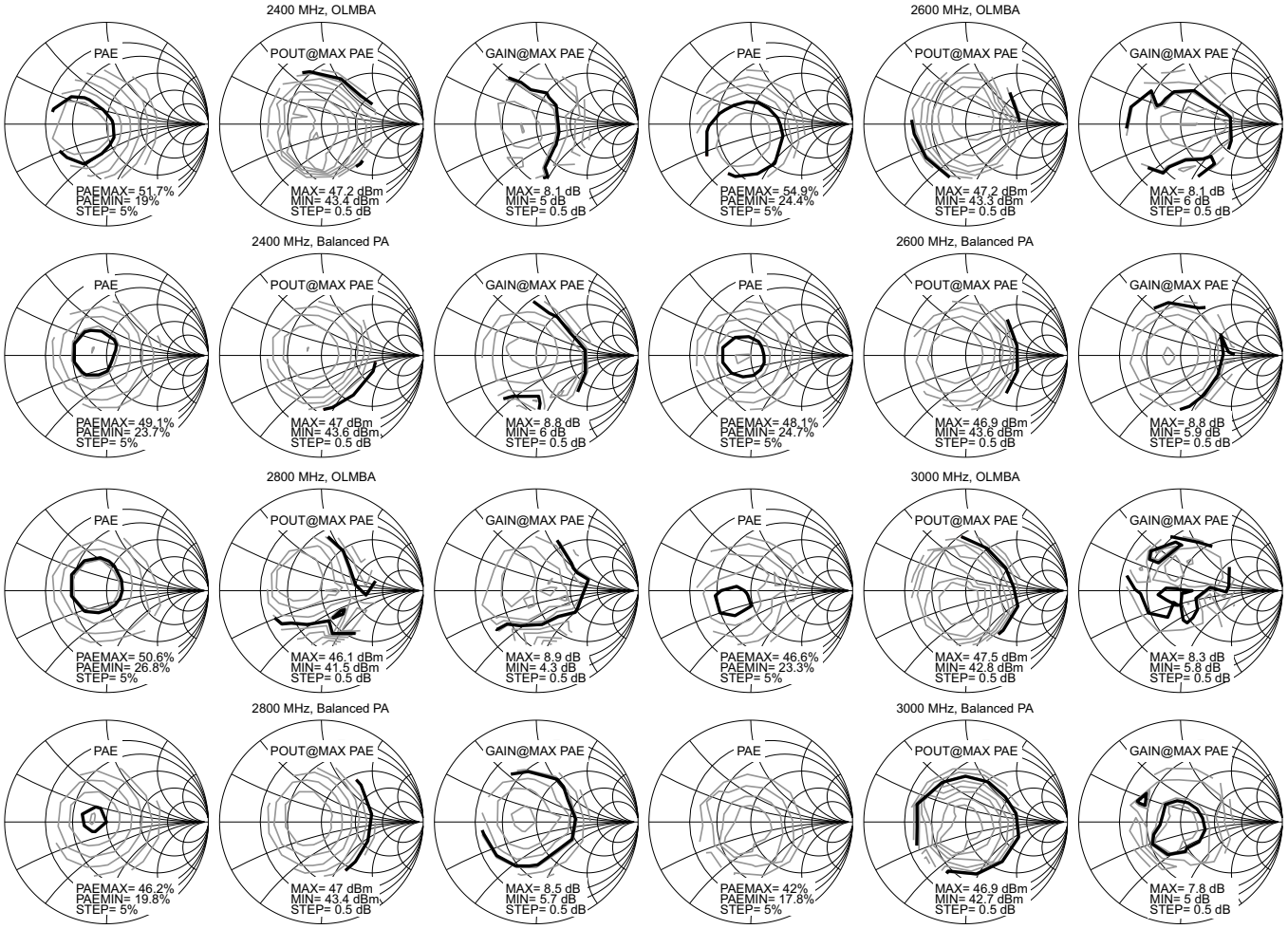

Fig. 20. OLMBA and balanced PA contours from 2200 to 3200 MHz, evaluated at maximum PAE point. Black thick contours highlight PAE of 45%, output power of 44 dBm, and gain of 7 dB. Grey thin contours limits and steps indicated in the legends.

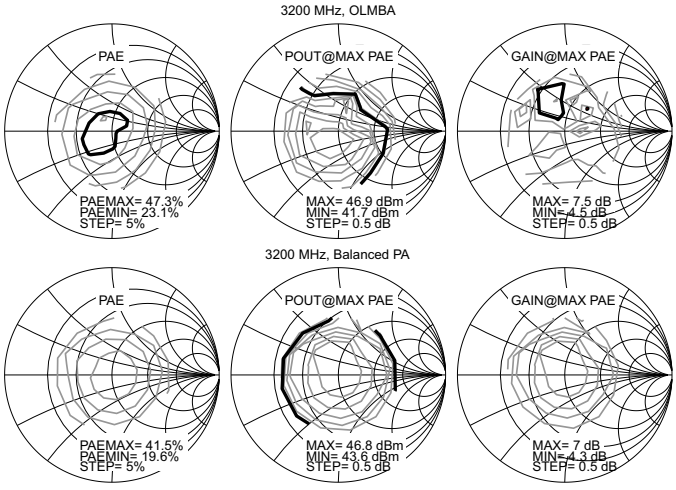

Fig. 21. OLMBA (top row) and balanced PA (bottom row) contours at 3200 MHz, evaluated at maximum PAE point. Black thick contours highlight PAE of 45%, output power of 44 dBm, and gain of 7 dB. Grey thin contours limits and steps indicated in the legends.

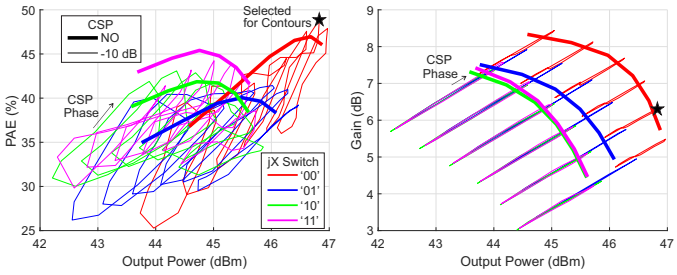

Fig. 22. PAE and gain vs. output power for the OLMBA prototype at 1.6 GHz, with $\Gamma_{\mathrm{L}} = 0.15\angle 30^{\circ}$. The results include all swept variables. The maximum PAE point used for contours is highlighted.

Expressions have been developed which describe the effect of the OLMBA control parameters on the reflection coefficients seen at the balanced amplifier devices; by comparison to the balanced amplifier case two noteworthy results have been highlighted – firstly that values of CSP control can be chosen which recover the balanced amplifier result under mismatch, but with no power dissipation in the isolation load, and secondly that values for both CSP and isolation termination can be chosen for any given mismatch which yield the same impedance at both balanced devices. This paper describes the realisation of a first demonstration of

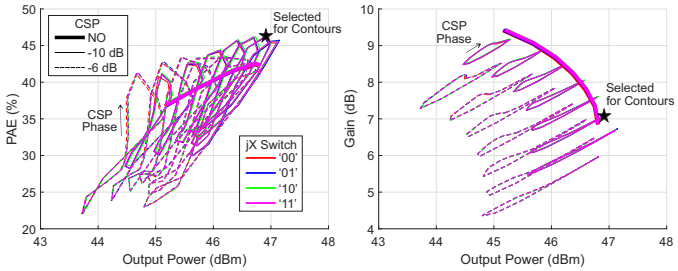

Fig. 23. PAE and gain vs. output power for the OLMBA prototype at 3 GHz, with $\Gamma_{\mathrm{L}} = 0.3^{\angle 195^\circ}$. The results include all swept variables. The maximum PAE point used for contours is highlighted.

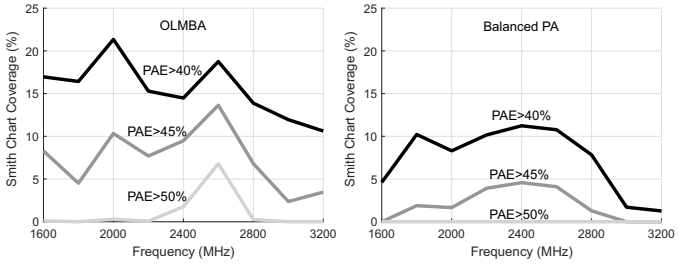

Fig. 24. Comparison OLMBA (left) vs. balanced PA (right) in terms of the Smith Chart area coverage for maximum PAE higher than a target, vs. measurement frequency.

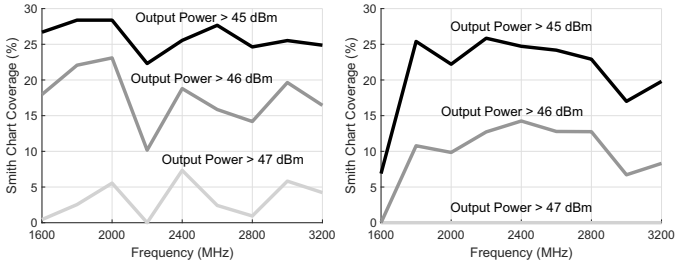

Fig. 25. Comparison OLMBA (left) vs. balanced PA (right) in terms of the Smith Chart area coverage for maximum output power higher than a target, vs. measurement frequency.

this technique using a design procedure based on manual iterative circuit design using control parameter optimisation. For the application targeted for the prototype, which is pulsed operation at saturation, the OLMBA can be electronically re-configured leading to better performance under load mismatch compared to an analogous balanced PA. This result offers a new architecture which designers can engineer for their particular applications and specifications when load mismatch is expected. This will include applications requiring efficient PAs at back-off although the demonstrated hardware has to date focussed on saturated conditions. It also opens a new design space for exploring further techniques for efficient amplification in antenna arrays, including for example feedback systems for automatically configuring the OLMBA parameters depending on the load impedance detected.

ACKNOWLEDGMENT

The authors would like to thank Focus Microwave and Mesuro Ltd for providing the passive impedance tuner and control software.

REFERENCES

[1] A. Keerti and A.-V. H. Pham, "RF characterization of SiGe HBT power amplifiers under load mismatch," *IEEE Trans. Microw. Theory Techn.*, vol. 55, no. 2, pp. 207–214, Feb. 2007.

[2] W. Fei, J. Su, G. Tingming, L. Jun, and S. Lingling, "RF characterization of GaAs HBT under load mismatch with real-time load-pull system," in *IEEE MTT-S Internat. Wirel. Symp. (IWS)*, Sep. 2020, pp. 1–3.

[3] A. Ghahremani, A.-J. Annema, and B. Nauta, "Load mismatch sensitivity of Class-E power amplifiers," *IEEE Trans. Microw. Theory Techn.*, vol. 67, no. 1, pp. 216–230, Jan. 2019.

[4] O. Hammi, J. Sirois, S. Boumaiza, and F. Ghannouchi, "Design and performance analysis of mismatched Doherty amplifiers using an accurate load-pull-based model," *IEEE Trans. Microw. Theory Techn.*, vol. 54, no. 8, pp. 3246–3254, Aug. 2006.

[5] O. Hammi, J. Sirois, S. Boumaiza, and F. M. Ghannouchi, "Study of the output load mismatch effects on the load modulation of Doherty power amplifiers," in *2007 IEEE Radio and Wireless Symposium*, Jan. 2007, pp. 393–394a.

[6] R. Quaglia and J. Lees, "Simplified analysis of the effect of load variation in common Doherty power amplifier architectures," in *2019 IEEE Topical Conference on RF/Microwave Power Amplifiers for Radio and Wireless Applications (PAWR)*, Jan. 2019, pp. 1–3.

[7] G. Wimpenny, J. Hildersley, T. Vlasits, S. Cummins, and N. Padfield, "Envelope tracking GaAs HBT PA performance characterization under high load mismatch conditions," in *2012 IEEE Topical Conference on Power Amplifiers for Wireless and Radio Applications*, Jan. 2012, pp. 37–40.

[8] E. Zenteno, M. Isaksson, and P. Händel, "Output impedance mismatch effects on the linearity performance of digitally predistorted power amplifiers," *IEEE Trans. Microw. Theory Techn.*, vol. 63, no. 2, pp. 754–765, Feb. 2015.

[9] R. Argaez-Ramirez, J.-R. Perez-Cisneros, and C. Fager, "Investigation of power amplifier performance under load mismatch conditions," in *IEEE Topic. Conf. on RF/Microw. Power Amplifiers for Radio and Wirel. Applic. (PAWR)*, Jan. 2021, pp. 41–43.

[10] J. Walker and M. Edwards, "Analyzing the VSWR withstand capability of a balanced amplifier," *Microwave Journal*, Oct. 2020.

[11] T. Nielsen, S. Lindfors, S. Tawfik, and T. Larsen, "Modeling power amplifiers with antenna mismatch," in *Proc. IEEE Intern. Symp. on Circ. and Syst.*, May 2005, pp. 5083–5086 Vol. 5.

[12] A. Suárez, F. Ramírez, and S. Sancho, "Generalized stability criteria for power amplifiers under mismatch effects," *IEEE Trans. Microw. Theory Techn.*, vol. 63, no. 12, pp. 4415–4428, Dec. 2015.

[13] A. Scuderi, A. Scuderi, F. Carrara, and G. Palmisano, "A VSWR-rugged silicon bipolar RF power amplifier," in *Proc. Bipolar/BiCMOS Circ. and Technol. Meeting.*, Oct. 2005, pp. 116–119.

[14] A. Scuderi, L. La Paglia, A. Scuderi, F. Carrara, and G. Palmisano, "A VSWR-protected silicon bipolar rf power amplifier with soft-slope power control," *IEEE J. Solid-State Circuits*, vol. 40, no. 3, pp. 611–621, Mar. 2005.

[15] M. van Heijningen, G. van der Bent, E. van der Houwen, A. Chowdhary, and F. van Vliet, "VSWR-protected 90 W L-band AlGaN/GaN power amplifier," in *IEEE MTT-S Int. Microw. Symp. Dig.*, Jun. 2014, pp. 1–3.

[16] J. Ferretti, S. Preis, W. Heinrich, and O. Bengtsson, "VSWR protection of power amplifiers using BST components," in *2016 German Microwave Conference (GeMiC)*, Mar. 2016, pp. 445–448.

[17] S. M. Bowers, K. Sengupta, K. Dasgupta, and A. Hajimiri, "A fully-integrated self-healing power amplifier," in *IEEE Radio Freq. integr. Circ. (RFIC) Symp.*, Jun. 2012, pp. 221–224.

[18] S. M. Bowers, K. Sengupta, K. Dasgupta, B. D. Parker, and A. Hajimiri, "Integrated self-healing for mm-wave power amplifiers," *IEEE Trans. Microw. Theory Techn.*, vol. 61, no. 3, pp. 1301–1315, Mar. 2013.

[19] J. Ponte, A. Ghahremani, M. Huiskamp, A.-J. Annema, and B. Nauta, "Theory and implementation of a load-mismatch protective class-e pa system," *IEEE Trans. Circuits Syst. I*, vol. 67, no. 2, pp. 369–377, Feb. 2020.

[20] S. Sinha, C. V. N. Rao, and D. Pujara, "Balanced power amplifier protection against load mismatch," *IEEE Microw. Wireless Compon. Lett.*, vol. 28, no. 2, pp. 165–167, Feb. 2018.

[21] P. Landin, O. Bengtsson, and M. Isaksson, "Power amplifier behavioural model mismatch sensitivity and the impact on digital predistortion performance," in *Proc. of Europ. Microw. Conf. (EuMC)*, Sep. 2009, pp. 338–341.

[22] H. Zargar, A. Banai, and J. C. Pedro, "A new double input-double output complex envelope amplifier behavioral model taking into account source and load mismatch effects," *IEEE Trans. Microw. Theory Techn.*, vol. 63, no. 2, pp. 766–774, Feb. 2015.
[23] J. Cai and J. B. King, "Behavioral model of RF PAs including load mismatch effects based on canonical section-wise piecewise-linear function," *IEEE Access*, vol. 8, pp. 9469–9479, Jan. 2020.
[24] A. van Bezooijen, C. Chanlo, and A. van Roermund, "Adaptively preserving power amplifier linearity under antenna mismatch," in *IEEE MTT-S Int. Microw. Symp. Dig.*, vol. 3, Jun. 2004, pp. 1515–1518 Vol.3.
[25] A. Mbaye, G. Baudoin, M. Villegas, and T. Gotthans, "Effect and adaptive correction of impedance mismatch between antenna and power amplifier on digital predistortion," in *2013 IEEE 11th International New Circuits and Systems Conference (NEWCAS)*, Jun. 2013, pp. 1–4.
[26] S. K. Dhar, A. Abdelhafiz, M. Aziz, M. Helaoui, and F. M. Ghannouchi, "A reflection-aware unified modeling and linearization approach for power amplifier under mismatch and mutual coupling," *IEEE Trans. Microw. Theory Techn.*, vol. 66, no. 9, pp. 4147–4157, Sep. 2018.
[27] L. Zhan, Y. Ouyang, G. Wu, B. Hu, and X. Zhang, "Linearization of power amplifiers with mismatched output impedance using on-line digital pre-distortion structure," *IEICE Electronics Express*, vol. 16, no. 9, pp. 1–3, Sep. 2019.
[28] A. Khodkumbhe, M. Huiskamp, A. Ghahremani, B. Nauta, and A.-J. Annema, "Preserving polar modulated Class-E power amplifier linearity under load mismatch," in *IEEE Radio Freq. integr. Circ. (RFIC) Symp.*, Aug. 2020, pp. 295–298.
[29] A. Brihuega, L. Anttila, and M. Valkama, "Neural-network-based digital predistortion for active antenna arrays under load modulation," *IEEE Microw. Wireless Compon. Lett.*, vol. 30, no. 8, pp. 843–846, Aug. 2020.
[30] A. Keerti and A. Pham, "Dynamic output phase to adaptively improve the linearity of power amplifier under antenna mismatch," in *IEEE Radio Freq. integr. Circ. (RFIC) Symp.*, Jun. 2005, pp. 675–678.
[31] Y. Yoon, H. Kim, K. Chae, J. Cha, H. Kim, and C.-H. Lee, "An antenna mismatch immuned CMOS power amplifier," in *Proc. IEEE Asian Solid-State Circ. Conf.*, Nov. 2010, pp. 1–4.
[32] D. Ji, J. Jeon, and J. Kim, "A novel load insensitive RF power amplifier using a load mismatch detection and curing technique," in *IEEE Radio Freq. integr. Circ. (RFIC) Symp.*, Jun. 2013, pp. 341–344.
[33] ——, "A novel load mismatch detection and correction technique for 3G/4G load insensitive power amplifier application," *IEEE Trans. Microw. Theory Techn.*, vol. 63, no. 5, pp. 1530–1543, May 2015.
[34] M. Alibakhshikenari, B. Virdee, L. Azpilicueta, C. See, R. Abd-Alhameed, A. Althuwayb, F. Falcone, I. Huyen, T. Denidni, and E. Limiti, "Analyzing the VSWR withstand capability of a balanced amplifier," *Scientific Reports*, no. 11, June. 2021.
[35] A. van Bezooijen, M. de Jongh, C. Chanlo, L. Ruijs, H. J. ten Dolle, P. Lok, F. van Straten, J. Sneep, R. Mahmoudi, and A. H. M. van Roermund, "rf-mems," in *IEEE Radio Freq. integr. Circ. (RFIC) Symp.*
[36] M. Alibakhshikenari, B. S. Virdee, A. A. Althuwayb, F. Falcone, and E. Limiti, "An innovative and simple impedance matching network using stacks of metasurface sheets to suppress the mismatch between antennas and rf front-end transceivers circuits," in *European Conf. on Antennas and Propag. (EuCAP)*, Mar. 2021, pp. 1–4.
[37] S. Hu, S. Kousai, and H. Wang, "Antenna impedance variation compensation by exploiting a digital Doherty power amplifier architecture," *IEEE Trans. Microw. Theory Techn.*, vol. 63, no. 2, pp. 580–597, Feb. 2015.
[38] A. Courty, P. Medrel, T. Reveyrand, P. Bouysse, J.-M. Nébus, and G. Soubercaze-Pun, "Analysis of load mismatch effect compensation in Doherty power amplifier," *Intern. Journ. of Microw. and Wir. Technol.*, vol. 13, no. 3, p. 211–222, Jun. 2021.
[39] N. S. Mannem, M.-Y. Huang, T.-Y. Huang, and H. Wang, "A reconfigurable hybrid series/parallel Doherty power amplifier with antenna VSWR resilient performance for MIMO arrays," *IEEE J. Solid-State Circuits*, vol. 55, no. 12, pp. 3335–3348, Dec. 2020.
[40] H. Lyu and K. Chen, "Balanced-to-Doherty mode-reconfigurable power amplifier with high efficiency and linearity against load mismatch," *IEEE Trans. Microw. Theory Techn.*, vol. 68, no. 5, pp. 1717–1728, Mar. 2020.
[41] C. F. Goncalves, F. M. Barradas, L. C. Nunes, P. M. Cabral, and J. C. Pedro, "Quasi-load insensitive Doherty PA using supply voltage and input excitation adaptation," *IEEE Trans. Microw. Theory Techn.*, vol. 70, no. 1, pp. 779–789, Jan. 2022.
[42] C. F. Gonçalves, F. M. Barradas, L. C. Nunes, P. M. Cabral, and J. C. Pedro, "Dynamic supply voltage control for PA output power correction under variable loading scenarios," *IEEE Trans. Microw. Theory Techn.*, vol. 69, no. 1, pp. 745–755, Jan. 2021.
[43] C. Sànchez-Pèrez, D. Sardin, M. Roberg, J. de Mingo, and Z. Popović, "Tunable outphasing for power amplifier efficiency improvement under load mismatch," in *IEEE MTT-S Int. Microw. Symp. Dig.*, Jun. 2012, pp. 1–3.
[44] K. Vivien, G. Baudoin, O. Venard, and P. Pierre-Charles-Felix, "A novel double balanced architecture with vswr immunity for high efficiency power amplifier," in *2019 IEEE International Conference on Microwaves, Antennas, Communications and Electronic Systems (COMCAS)*, Nov. 2019, pp. 1–5.
[45] D. J. Collins, R. Quaglia, J. R. Powell, and S. C. Cripps, "The orthogonal LMBA: A novel RFPA architecture with broadband reconfigurability," *IEEE Microw. Wireless Compon. Lett.*, vol. 30, no. 9, pp. 888–891, Sep. 2020.
[46] D. J. Shepphard, J. Powell, and S. C. Cripps, "An efficient broadband reconfigurable power amplifier using active load modulation," *IEEE Microw. Wireless Compon. Lett.*, vol. 26, no. 6, pp. 443–445, Jun. 2016.
[47] P. H. Pednekar, E. Berry, and T. W. Barton, "RF-Input load modulated balanced amplifier with octave bandwidth," *IEEE Trans. Microw. Theory Techn.*, vol. 65, no. 12, pp. 5181–5191, Dec. 2017.
[48] R. Quaglia and S. Cripps, "A load modulated balanced amplifier for telecom applications," *IEEE Trans. Microw. Theory Techn.*, vol. 66, no. 3, pp. 1328–1338, Mar. 2018.
[49] J. R. Powell, D. J. Shepphard, R. Quaglia, and S. C. Cripps, "A power reconfigurable high-efficiency X-band power amplifier MMIC using the load modulated balanced amplifier technique," *IEEE Microw. Wireless Compon. Lett.*, vol. 28, no. 6, pp. 527–529, Jun. 2018.
[50] J. Pang, Y. Li, M. Li, Y. Zhang, X. Y. Zhou, Z. Dai, and A. Zhu, "Analysis and design of highly efficient wideband RF-input sequential load modulated balanced power amplifier," *IEEE Trans. Microw. Theory Techn.*, vol. 68, no. 5, pp. 1741–1753, May 2020.
[51] Y. Cao and K. Chen, "Pseudo-Doherty Load-Modulated Balanced Amplifier with wide bandwidth and extended power back-off range," *IEEE Trans. Microw. Theory Techn.*, vol. 68, no. 7, pp. 3172–3183, Jul. 2020.
[52] J. Pang, C. Chu, Y. Li, and A. Zhu, "Broadband RF-input continuous-mode load-modulated balanced power amplifier with input phase adjustment," *IEEE Trans. Microw. Theory Techn.*, vol. 68, no. 10, pp. 4466–4478, Oct. 2020.
[53] Y. Cao, H. Lyu, and K. Chen, "Asymmetrical Load Modulated Balanced Amplifier with continuum of modulation ratio and dual-octave bandwidth," *IEEE Trans. Microw. Theory Techn.*, vol. 69, no. 1, pp. 682–696, Jan. 2021.
[54] C. Chu, T. Sharma, S. K. Dhar, R. Darraji, X. Wang, J. Pang, and A. Zhu, "Waveform engineered sequential load modulated balanced amplifier with continuous class-F^1 and class-J operation," *IEEE Trans. Microw. Theory Techn.*, vol. 70, no. 2, pp. 1269–1283, Feb. 2022.
[55] H.-C. Chang, P. Roblin, Y. Hahn, J. I. Martinez-Lopez, C. Liang, and K. Rawat, "Frequency-agile class-J power amplifier with clockwise fundamental- and second-harmonic loads," *IEEE Trans. Microw. Theory Techn.*, vol. 68, no. 7, pp. 3184–3196, Jul. 2020.
[56] S. Cripps, *RF power amplifiers for wireless communications*, ser. Artech House Microwave Library. Artech House, 2006.

Roberto Quaglia was born in Casale Monferrato, Italy, in 1984. He graduated *cum laude* in electronic engineering from Politecnico di Torino in 2008. In 2012, he received the Ph.D. degree in electronic devices from the Politecnico di Torino, Turin, Italy. His research interests concern the design, modeling and predistortion of high efficiency MMIC power amplifiers, and he is currently a Lecturer at the School of Engineering of Cardiff University. He is a member of the IEEE MTT-TC 12. Dr. Quaglia was the recipient of a European Union Marie Skłodowska Curie fellow in 2015, and of the 2009 Young Graduated Research Fellowship presented by the GAAS Association.

Jeffrey Powell received BSc and PhD degrees from the University of Birmingham in the UK in 1992 and 1995 respectively. Following graduation he continued work at Birmingham investigating properties of ferroelectric and superconducting materials at microwave frequencies. From 2001 to 2010 he worked as a principal engineer at QinetiQ in the UK where he performed many MMIC circuit, hybrid and module designs for many applications from 2 to 110 GHz using a wide range of commercial and research-based circuit and packaging technologies. In 2010 he formed Skyarna Ltd, a design consultancy which specialises in the design of leading edge circuits; including wideband high efficiency amplifiers and active circuits to 300 GHz. He has contributed to over 50 journal and conference publications and also 4 patent applications. Dr Powell was co-recipient of the *2018 IEEE Microwave and Wireless Component Letters Tatsuo Itoh Best Paper Award*.

Kauser A. Chaudhry received his MSc (2001) in Microwave and Opto-electronics from University College London (UCL). He has recently completed his PhD at Cardiff University where he is working as a researcher.in the field of PA design and characterisation for the emerging base station and microwave heating applications. Dr Chaudhry has over 15 years of industrial experience, working for companies like Nokia, Panasonic and NXP Semiconductors.

Prof. Steve Cripps (M'81-SM'90-F'11-LF'16) received the master's and Ph.D. degrees from Cambridge University, Cambridge, U.K., in 1975. He spent many years working within the high frequency ("microwave") electronics industry in the U.K. and the USA. He was a Designer, a Manager, and an Independent Consultant. He is currently a Distinguished Research Professor with Cardiff University, Wales, U.K. He has authored several books on RF Power Amplifiers. Dr. Cripps was a recipient of the 2008 IEEE Microwave Applications Award and the 2015 Microwave Prize. He served as an Associate Editor for IEEE MICROWAVE AND WIRELESS COMPONENTS LETTERS.